Supporting Information

Contradictory role of reactive oxygen species in dissolution-dependent activity of Pb-based anodes in acidic electrooxidation

Siwei Zhuang [a,b], Ning Duan [a,b], Linhua Jiang [a,b], Feilong Zhang [c], Fuyuan Xu [a,b*]*

[a]State Key Laboratory of Pollution Control and Resources Reuse, College of Environmental Science and Engineering, Tongji University, Shanghai, 200092, China.

[b]Shanghai Institute of Pollution Control and Ecological Security, Shanghai, 200092, China.

[c]School of Environment, Tsinghua University, Beijing 100084, China.

***Corresponding author:**

Ning Duan (ningduan@tongji.edu.cn)

Fuyuan Xu (fuyuanxu@tongji.edu.cn)

Table of content:

Supplementary methods:

Text S1. Synthesis of anode samples

The lead substrate was encapsulated in a semi-enclosed polymethyl methacrylate device to ensure that only its front face (1 cm^2) was exposed to electrolyte. A strict pretreatment process should be adopted: Ultrasonic cleaning, polishing and deionized water cleaning were performed to minimize the influence of lead passivation products on sample preparation. The PMA samples was obtained via a simple electrodeposition process using a high-purity graphite plate and lead substrate as cathode and anode.The target MnO_2 layer were prepared at a constant current density of 5 mA cm^{-2} and a temperature of 90°C in the electrolytes containing 40 g L^{-1} Mn^{2+} and 40 g L^{-1} H_2SO_4. The SPPA samples were prepared at a different condition: 50 mA cm^{-2}, 45°C, 160 g L^{-1} H_2SO_4, and adopted aluminum plate as a cathode.

Text S2. Morphological characterization of anode samples

The phase transition of anode samples was recorded with an X-ray diffractometer (XRD, D-max/3C) at a scan rate of 0.02 ° s^{-1}. According to the comparison results of the XRD patterns and the JCPDS cards, the crystal plane with the highest diffraction peak enlargement ratio was identified as the main exposed crystal plane. The surface morphologies of different samples were compared using scanning electron microscopy (SEM, ZEISS Gemini 300) equipped with an energy-dispersive X-ray (EDX) detector[1]. High-resolution transmission electron microscope (HRTEM) analyses were carried out by a JEOL JEM-F200 microscope. The surface element

distribution was recorded by using an X-ray photoelectron spectrometer[2], and binding energies were calibrated against the C1s signal at 284.60 eV of adventitious hydrocarbons.

Text S3. Calculation of voltammetric charge (*q)**

The voltammertric charge (*q**) of cyclic voltammetry (CV) curves was calculated under integral conversion method (1).

$$q^* = it = \frac{\int_{V1}^{V2} idV}{v} \quad (1)$$

wherein i is current density; V_n (n=1, 2) is the marker points of the oxidation section of the scanning curves; v is canning rate.

Figures:

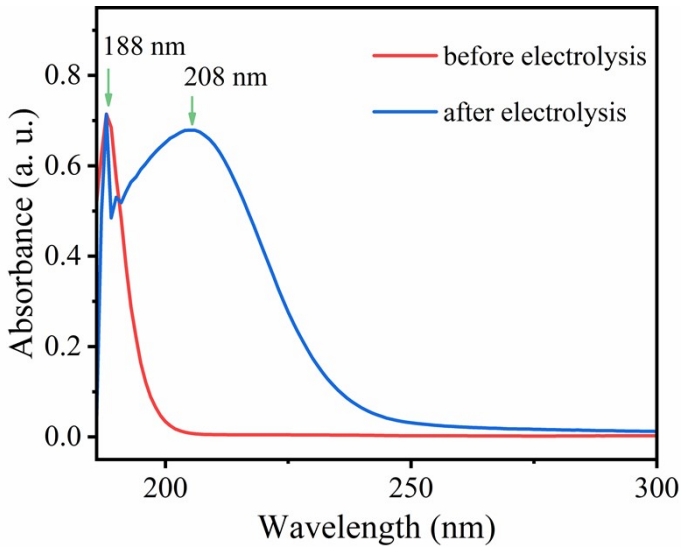

Figure S1. UV-vis spectra of electrolyte samples before and after electrolysis with using H_2SO_4 electrolytes as the base solution.

The clearly readable peaks centered at 188 and 208 nm of UV-vis spectra can be assigned to SO_4^{2-} and Pb^{2+} in electrolyte samples, respectively. The Pb^{2+} dissolution can be calculated based on the peak intensity.

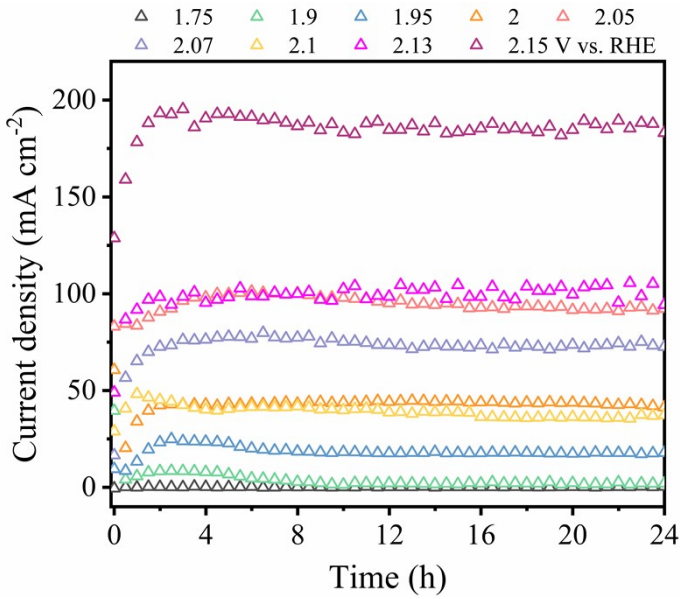

Figure S2. Current density versus time profile of Pb-based anodes at different anode potentials.

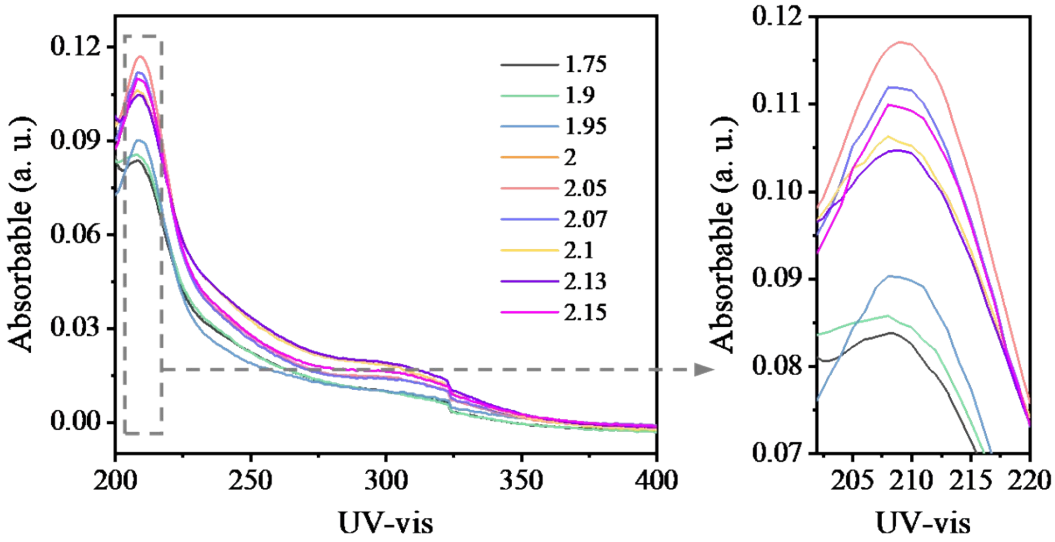

Figure S3. UV-vis spectra of the used electrolytes at different anode potentials.

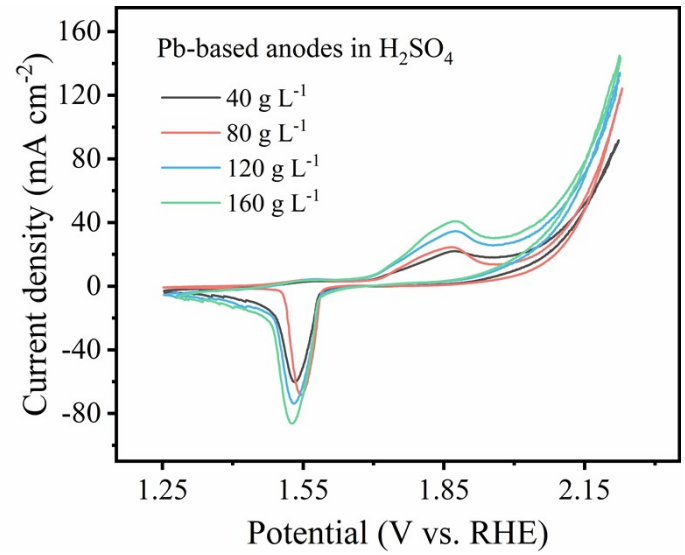

Figure S4. The CV curves of Pb-based anodes in solutions with different H_2SO_4 concentration.

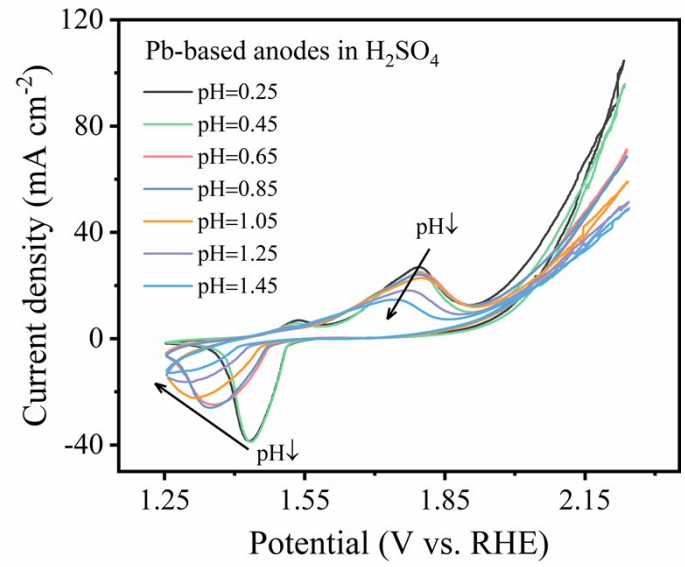

Figure S5. The CV curves of Pb-based anodes in solutions with different pH. The pH value of electrolytes was controlled through NaOH addition.

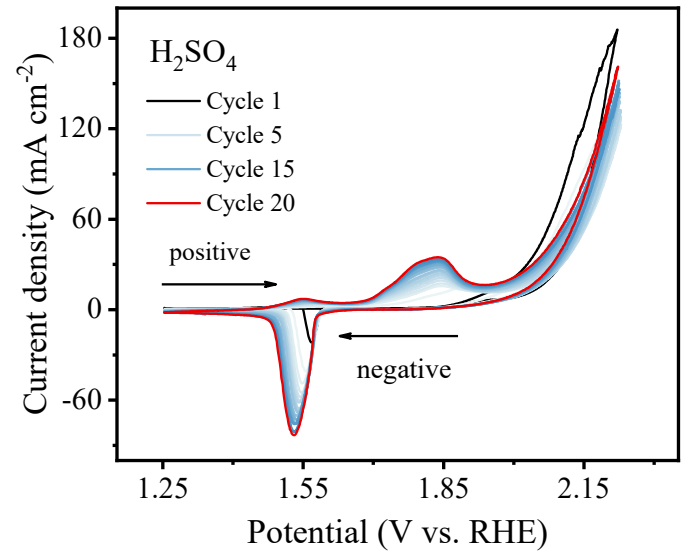

Figure S6. Cyclic voltammograms of Pb-based anode in the sulfuric acid-containing electrolyte (160 g L^{-1} H_2SO_4). Tests were cycled 20 times with a scan rate of 10 mV s^{-1}.

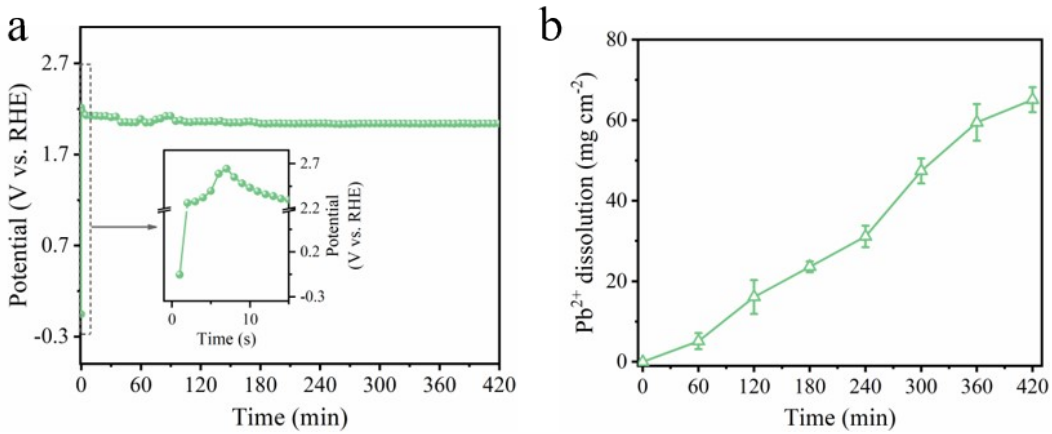

Figure S7. (**a**) Anode potential and (**b**) Pb dissolution summary of the Pb-based anodes in extreme corrosion conditions (160 g L^{-1} H_2SO_4) over chronopotentiometry tests at 50 mA cm^{-2}.

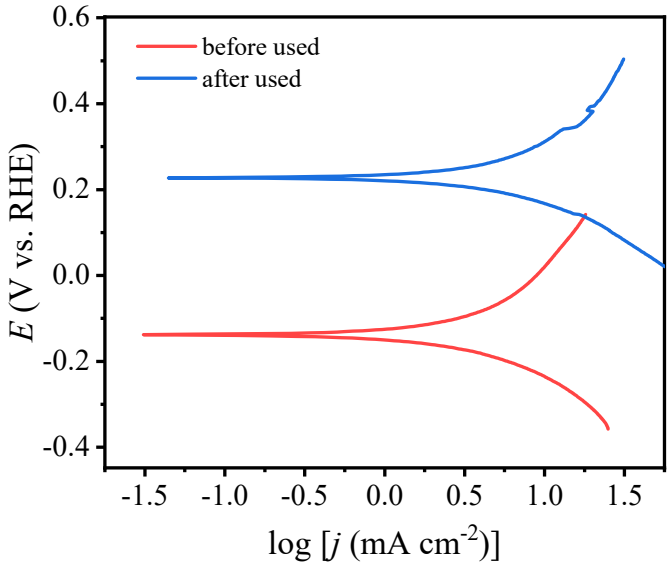

Figure S8. Tafel slopes of Pb-based anodes before and after use under chronopotentiometry tests in 160 g L^{-1} H_2SO_4 electrolytes.

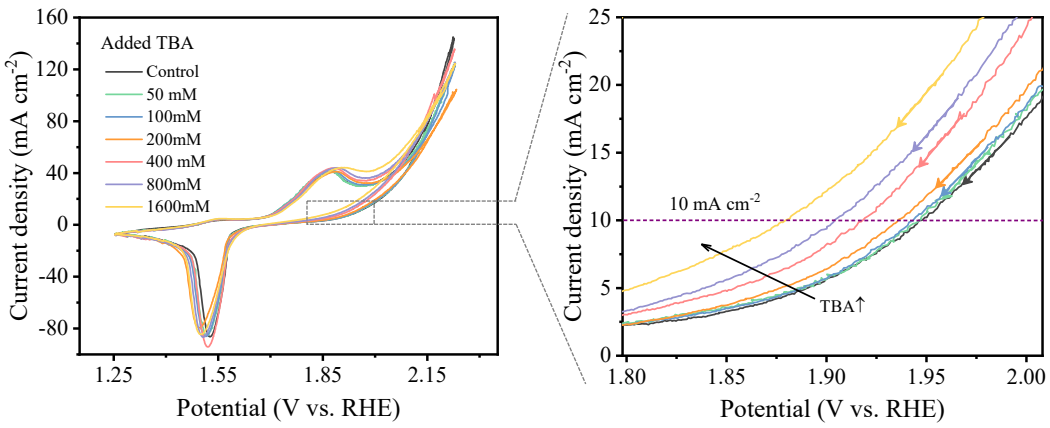

Figure S9. Effect of the TBA concentration on the electrooxidation behavior of Pb-based anodes in H_2SO_4 electrolytes.

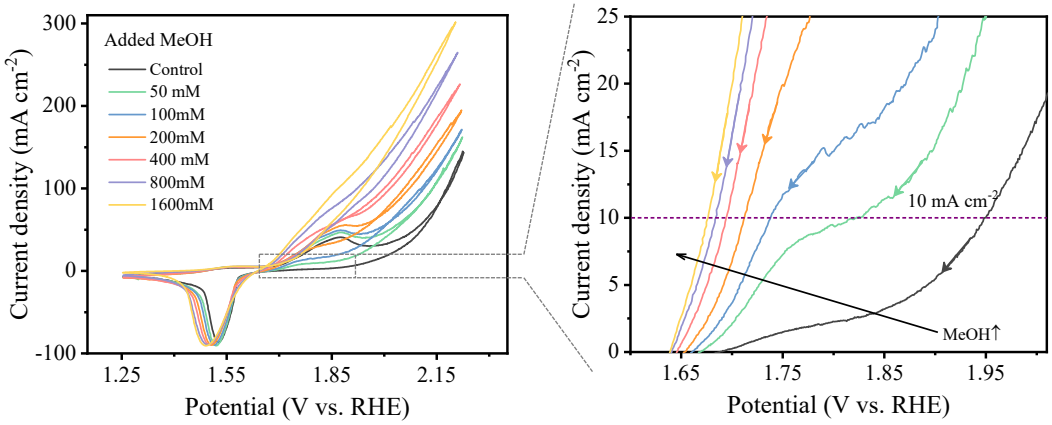

Figure S10. Effect of the MeOH concentration on the electrooxidation behavior of Pb-based anodes in H_2SO_4 electrolytes.

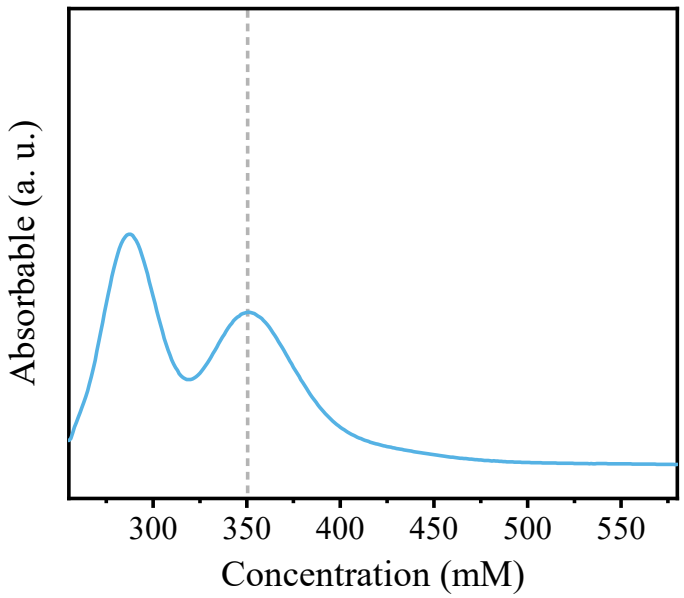

Figure S11. UV-vis spectra of used H_2SO_4 electrolytes in cyclic voltammogram test using Pb-based anodes.

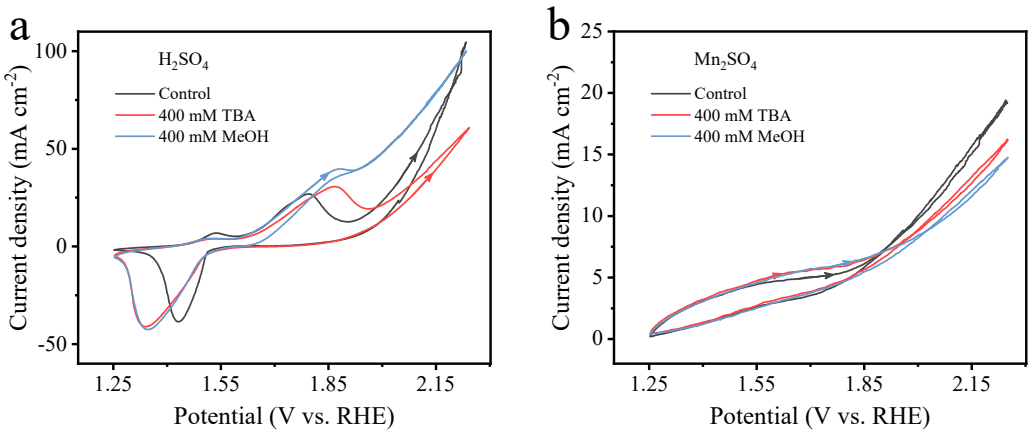

Figure S12. Cyclic voltammograms of Pb-based anode in (**a**) H_2SO_4 and (**b**) $MnSO_4$ electrolytes without and with adding TBA or MeOH.

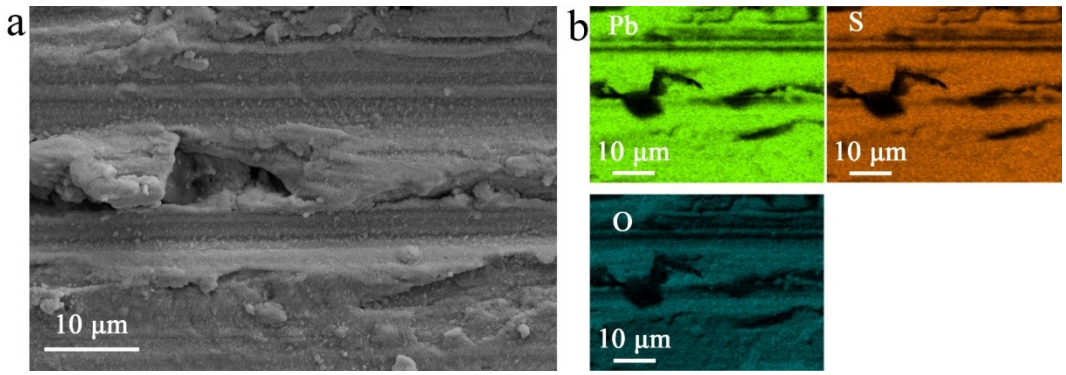

Figure S13. (**a**) The SEM image of SPPA. (**b**) The EDX element mapping of Pb, S and O.

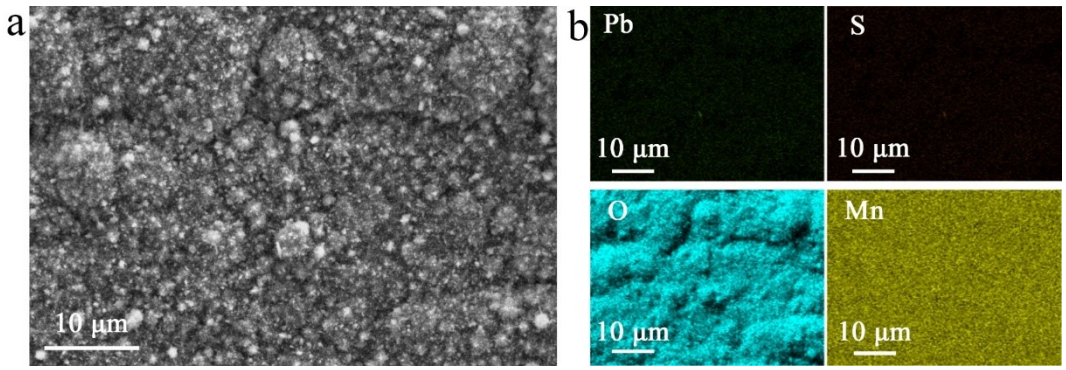

Figure S14. (**a**) The SEM image of PMA. (**b**) The EDX element mapping of Pb, S and O.

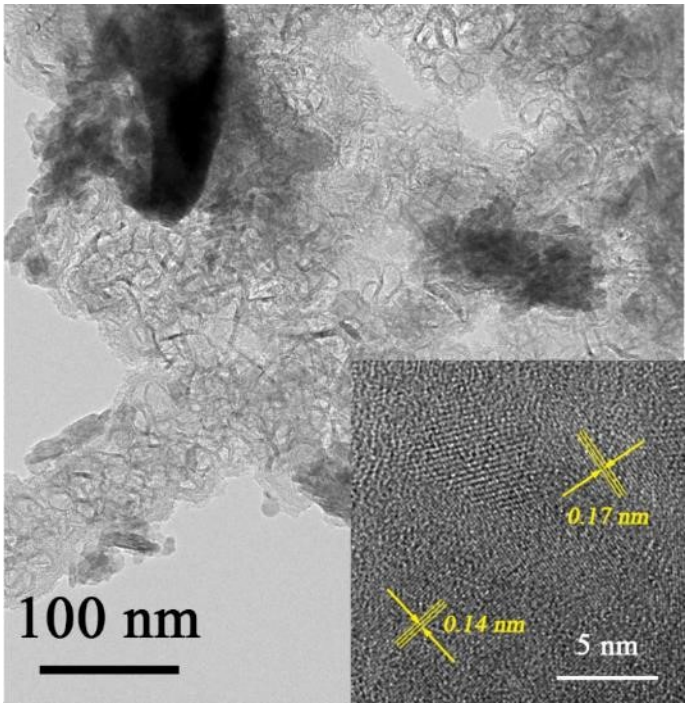

Figure S15. HRTEM images of MnO_2 particles at different magnifications.

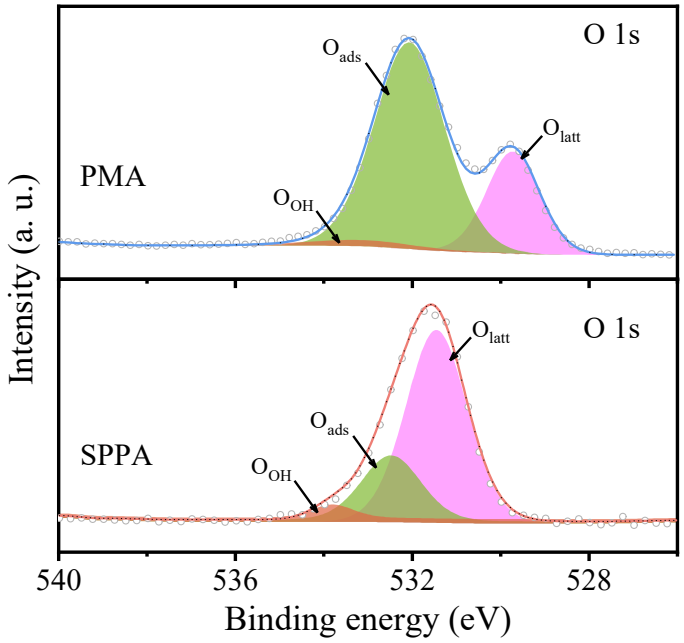

Figure S16. High-resolution XPS spectra of the SPPA and PMA anodes for O 1s.

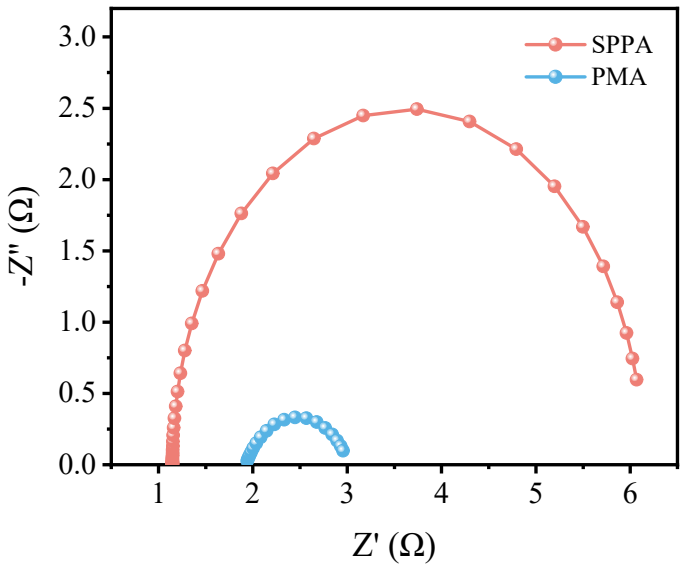

Figure S17. EIS plots of the SPPA and PMA samples at an anodic polarization potential of 1.95 V vs. RHE.

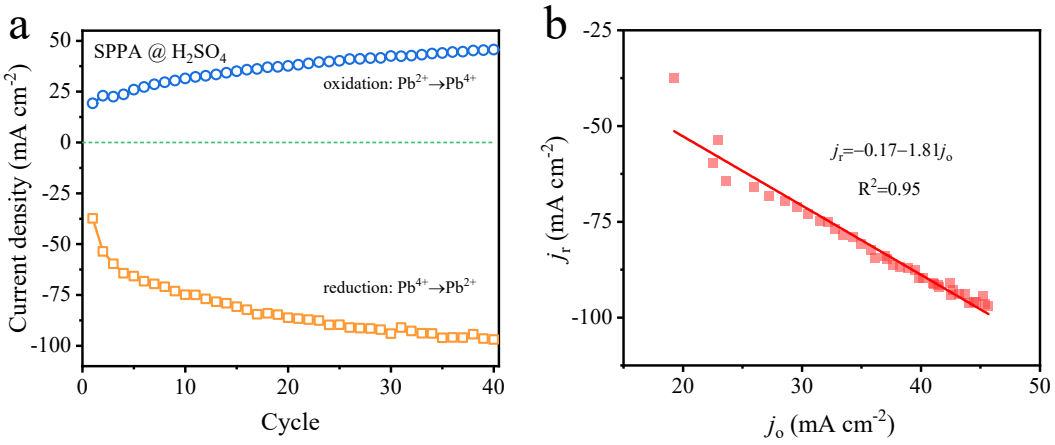

Figure S18. (**a**) Responses of SPPA to anode oxidation (j_o, blue line) and anode reduction (j_r, orange line). (**b**) Anode corrosion trends of j_r as a function of j_o for SPPA.

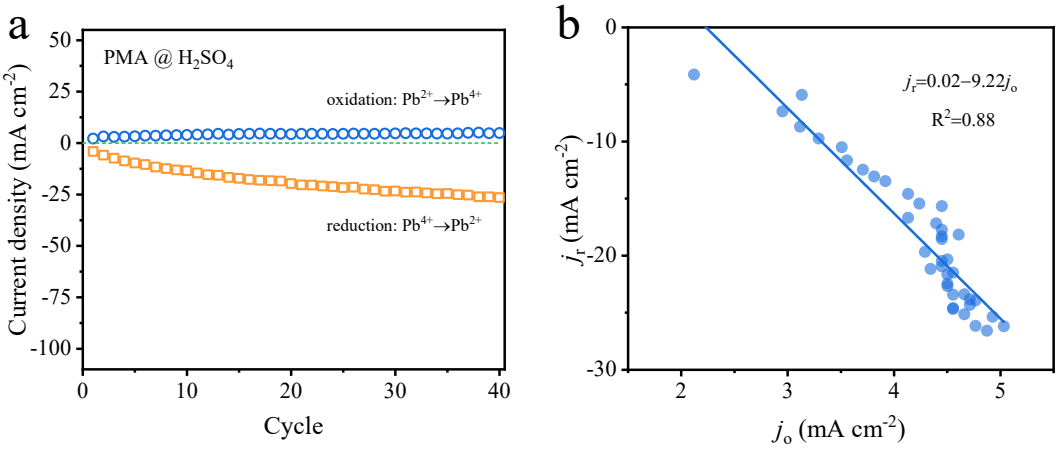

Figure S19. (**a**) Responses of PMA to anode oxidation (j_o, blue line) and anode reduction (j_r, orange line). (**b**) Anode corrosion trends of j_r as a function of j_o for PMA.

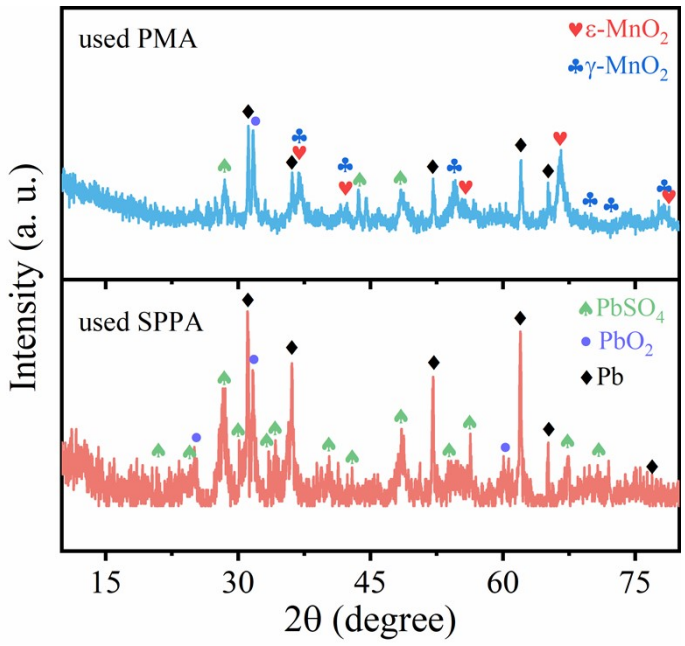

Figure S20. XRD patterns of the SPPA and used PMA samples after chronopotentiometry test.

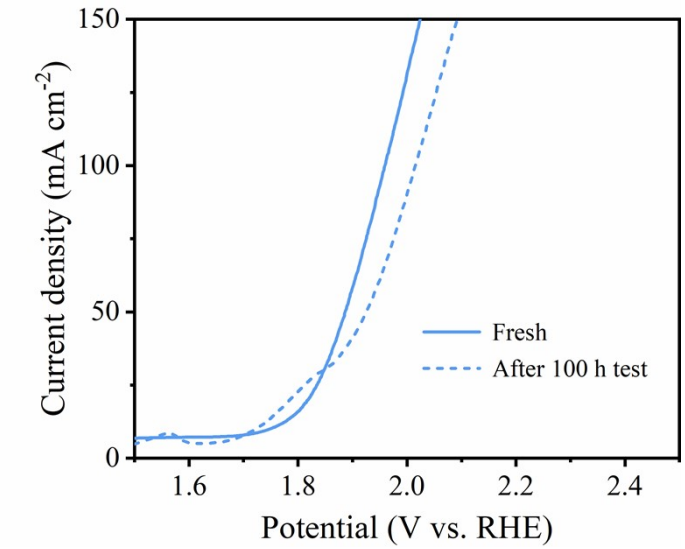

Figure S21. Stability of PMA in the long-term running chronopotentiometry test in 160 g L^{-1} H_2SO_4 electrolytes.

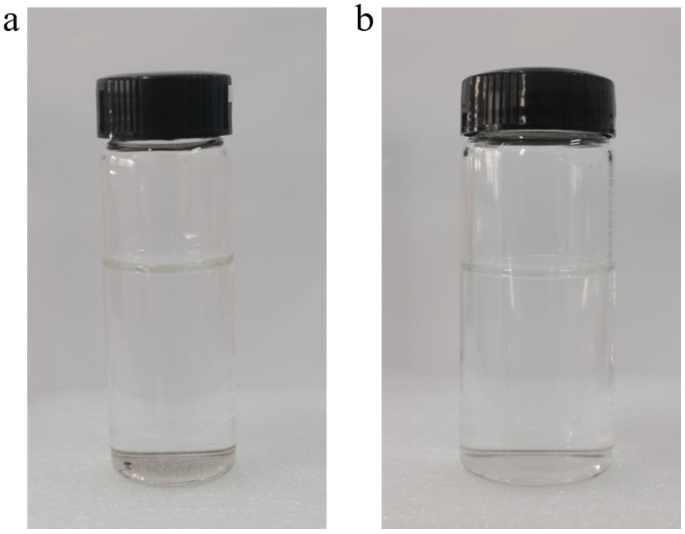

Figure S22. Photographs of the electrolyte samples after chronopotentiometry test using (**a**) SPPA and (**b**) PMA anodes.

Tables:

Table S1. XPS analysis of the as-fabricated SPPA and PMA samples.

Sample		SPPA	PMA
Mn 2p	Mn^{4+} (%)		24.52
	Mn^{3+} (%)		72.63
	Mn^{2+} (%)		2.85
Pb 4f	Pb^{4+} in PbO_2 (%)	2.36	4.78
	Pb^{2+} in PbO_2 (%)	2.70	28.16
	Pb^{2+} in $PbSO_4$ (%)	94.94	67.06
O 1s	O_{latt} (%)	26.31	60.86
	O_{ads} (%)	70.51	25.19
	O_{OH} (%)	3.18	13.95
Mn/Pb		0	52.1
S/Pb		0.85	1.64

Table S2. EO performance of SPPA and PMA in acidic electrolytes (160 g L^{-1} H_2SO_4).

Indexes	SPPA	PMA
η_{10} (mV)	756	536
Tafel slope (mV dec^{-1})	177.6	97.7
Lead oxidation (mA cm^{-2})	45.7	4.9
Lead reduction (mA $cm^{-2)}$	-97.0	-26.6
q* (C cm^{-2})	4.1	12.1

Supplementary References:

1. J. Li, J. Hu, M. Zhang, W. Gou, S. Zhang, Z. Chen, Y. Qu and Y. Ma, *Nat. Commun.*, 2021, **12**, 3502.
2. L. Mu, Y. Wang and W. A. Tarpeh, *ACS Sustain. Chem. Eng.*, 2020, **8**, 8648-8654.